Eur. Phys. J. Special Topics **xxx**, xxx–xxx (2020)

https://doi.org/10.1140/epjst/e2020-000244-4

THE EUROPEAN PHYSICAL JOURNAL SPECIAL TOPICS

Regular Article

Mechanism of unipolar electromagnetic pulses emitted from the hypocenters of impending earthquakes

Friedemann T. Freund[1,2,3,a], Jorge Arturo Heraud[4], Victor A. Centa[4], and John Scoville[1]

[1] GeoCosmo Science and Research Center, Los Altos, CA 94024, USA
[2] NASA Ames Research Center, Code SCR, Moffett Field, CA 94035-1000, USA
[3] San Jose State University, Department of Physics, San Jose, CA 95192-0106, USA
[4] Pontificia Universidad Catolica del Peru (PUCP), Lima, Peru

Received 2 October 2020 / Accepted 7 October 2020
Published online (Inserted Later)

Abstract. Unipolar pulses (UPs) are short events characterized by outbursts of electromagnetic (EM) energy from deep within the Earth's crust. First recognized prior to the 2007 $M = 5.4$ Alum Rock earthquake in northern California, UPs can be as short as 150 ms, followed by an overshoot in the opposite polarity direction or by undulations of the EM field lasting from to 2–20 sec. Near Lima, Peru, and Tacna, Peru, thousands of UPs in the 1–3 nT intensity range have been recorded, emitted from the 25–65 km depth range, thought to arise in patches at the top of the Benioff Zone of the subducting Nazca Plate. To understand how these EM pulses can be generated deep in the rock column, we consider that rocks contain peroxy defects, typically O_3Si–OO–SiO_3, which, when subjected to increasing deviatoric stresses, break up in two steps. Step I: electrons in the tight non-bonding π^{nb} molecular orbital decouple by transitioning into the antibonding σ^*-level, where they occupy a significantly larger volume. This volume expansion is possible only, when the internal pressure in the stressed subvolume overcomes its confining pressure. This in turn requires that the number density of peroxy defects in the rock is high enough so that, during the $\pi^{nb} \rightarrow \sigma^*$ transition of the O^-–O^- bonds, the wave function of their decoupled O^- states overlap, causing a solid plasma state with an internal electron degeneration pressure that can force the volume expansion against the load of the overlying rock column. Step II: once the σ^*-level is reached, the decoupled O^-–O^- bonds can dissociate, generating highly mobile charge carriers, electrons e' and holes $h^\bullet$, which can burst out the stressed subvolume causing it to instantly contract again. Thus, UPs appear to be linked to an explosive expansion of stressed subvolumes of rocks against their lithostatic overload, followed by an outburst of electronic charge carriers and concomitant volume contraction.

[a] e-mail: friedemann.t.freund@nasa.gov

1 Introduction

Earthquakes are cataclysmic mechanical events that generate P and S waves. As the seismic waves propagate, the S waves have been observed to trigger outbursts of light from the ground, so-called "earthquake lights" (EQL), that typically last only for a fraction of a second. EQLs have been reported for a long time. They can occur both during earthquakes, e.g. while the seismic waves propagate, and hours, days, even weeks before major seismic events [1–6]. One line of thought is that these flashes of light may be caused by combustible gases released from the ground, self-igniting due to phosphine [7]. An alternative explanation invokes electric discharges bursting through the Earth's surface [8]. Such sudden electric discharges seem to also occur inside the rock column, without breaking through the Earth surface. They are probably the source of unipolar pulses (UPs) that consist of EM emissions from some source or sources deep below the Earth's surface [9,10]. These EM outbursts appear to come from rock volumes that are subjected to periods of increasing tectonic stresses [11].

Telluric currents, also known as Earth currents, flow in the Earth crust and upper mantle [12,13]. They wax and wane on time scales of hours to days and weeks, also months to years. Like any currents that flow, telluric currents produce a magnetic field [14]. As they fluctuate, they radiate electromagnetic (EM) waves [14]. This paper addresses a particular form of EM signals, which has not yet been widely studied: short unipolar pulses (UPs) emitted from deep within the rock column, apparently related to the build-up of tectonic stresses, typically recorded a few days to a few weeks before major earthquakes [15].

A *conditio sine qua non* for any electric currents is the availability of mobile charges that can move in response to some thermodynamic driving force. These charges may be ionic in nature (cations or anions) or electronic in nature (electrons or defect electrons, the latter also known as holes). This report focuses the processes by which powerful telluric currents may be generated in the rock column [16]. Two situations can be distinguished:

1. Mobile charge carriers already exist under the given temperature (T) and pressure (P) conditions, but only need an electric potential to flow and produce a current;
2. Mobile charge carriers do not exist under the given T and P conditions but can suddenly become activated by stress to release mobile charge carriers where none existed before.

In the shallow part of the crust, in the range of 0 to 5–7 km depth, rocks typically retain some interconnected porosity with water saturating the intergranular space [17,18]. This water contains dissolved cations and anions. Hence, ionic charge carriers are available to generate electrolytical currents when, for instance, geomagnetic activity in the ionosphere induces electric fields into the Earth crust, which provide the necessary driving force. Alternatively, when water is forced to flow through porous rocks along stress gradients, the cations dissolved in the pore water tend to be preferentially retained on the walls of the pores, while the anions are carried along with the water flow. This leads to charge separation and streaming potentials and, hence, electrokinetic potentials that lead to currents, which are called streaming currents [6,19].

The seismogenic zone, where most earthquakes occur [20,21], extends from about 7–10 km to 45 km or deeper along subduction zones. In this depth range, rocks cannot sustain open porosity, even over geologically short time scales [22]. This fact rules out stress-activated fluid flow and, hence, streaming currents. At the same time the temperatures in this depth range are moderate, well below magmatic. Hence, the rocks are still poor ionic conductors [23] and any EM signals observed cannot be due to ionic conductivity in the solid state.

However, the rocks in this depth range – mostly gabbro, granite, anorthosite etc. – contain defects that are normally electrically inactive but can activate highly mobile electronic charge carriers when perturbed by tectonic stresses. The defects in question consist of pairs of oxygen anions that have converted from their usual 2-valence state to the 1-valence state. They form peroxy bonds, O^-–O^- such as in O_3Si–OO–SiO_3, where Si^{4+} may be substituted by Al^{3+} or other trivalent cations [14]. Peroxy defects occur inside the matrix of the constituent mineral grains but also along grain boundaries. Those along grain boundaries, especially those that straddle across grain boundaries, will be particularly sensitive to activation by mechanical stress. The reason is that any ever so slight shifting of mineral grains relative to each other will break peroxy bonds and generate two types of electronic charge carriers, electrons e' and holes $h\bullet$, which have finite lifetimes [24]. The mechanical process applies to the seismogenic depth range [25–27]. The electrons e' are confined to the rock volume experiencing dynamic stresses, while the holes $h\bullet$ have the ability to flow out of the stressed rock volume into and through the surrounding less stressed or unstressed rocks [28].

Under certain special conditions, however, both e' and $h\bullet$ appear to be able to burst out together from stressed subvolumes of rocks. At least this is what the very short EM pulses seem to tell us known as unipolar pulses, UPs [29]. UPs were first noted in magnetometer traces recorded prior to the $M = 5.4$. Alum Rock earthquake of Oct. 30, 2007 in northern California, a strike-slip event with a hypocentral depth of 9.6 km [10]. A Zonge 3-axis search-coil magnetometer, capable of detecting EM signals down to the picoTesla (pT) range, had been set up as part of the Californian QuakeFinder stations network about 2 years before the Alum Rock event, fortuitously less than 2 km from the future epicenter. The UPs occurred in the 0.01–12 Hz band and consisted of an increasing number of short duration (1 to 30 s duration) pulsations that peaked about 13 days prior to the seismic event. The amplitudes of the pulses, 3–20 nT, were well above to the ambient noise at this site 10–250 pT. They typically lasted 150 msec, rising sharply and decaying slightly more slowly. Such high signal intensities point to powerful current bursts, in the range of 10^4–10^5 A at their points of origin [30]. The number of UPs increased with time from 5–10 to more than 200 per 24 hr. Their unipolar signature rules out that they were emitted from a point source. Instead they must have been emitted from a linear or planar source volume [31].

Since the Alum Rock events, UPs have been recorded at other locations, most notably in Peru, where a network of 3-axis search-coil Zonge magnetometers has been set up along the Pacific Coast [32]. There too the UPs consist of abrupt EM emission events of positive polarity, lasting about 150 msec, occasionally followed by an overshoot into the negative polarity regime before returning to the background level. Figure 1a shows an overlay of thousands of pulses recorded at the Tacna Station in southern Peru. They consistently last for ∼150 msec and are followed by a slight overshoot to negative polarity and slow return to the baseline.

Figure 1b compiles 5644 pulses received between February 1, 2013 and August 16, 2018 at the San Lorenzo Island station off the coast of Lima, Peru, where two 3-axis search coil magnetometers are being used to triangulate the points of origin of these UPs. The histogram in Figure 1c documents that the majority of the pulses recorded at this station fall into the 100–150 msec bracket. They are typically followed by low amplitude fluctuations that can last 2–3 sec, occasionally as long as 10–20 sec. Triangulation shows that the UPs originate from the Benioff Zone of the subducting Nazca Plate, which drags down a small submarine ridge. The UPs are emitted between 25 to 65 km depth. They tend to occur in clusters of a dozen or more, emitted within hours of each other. The clusters are separated by a few days and characteristically followed by earthquakes in the 3–4.5 magnitude range at the

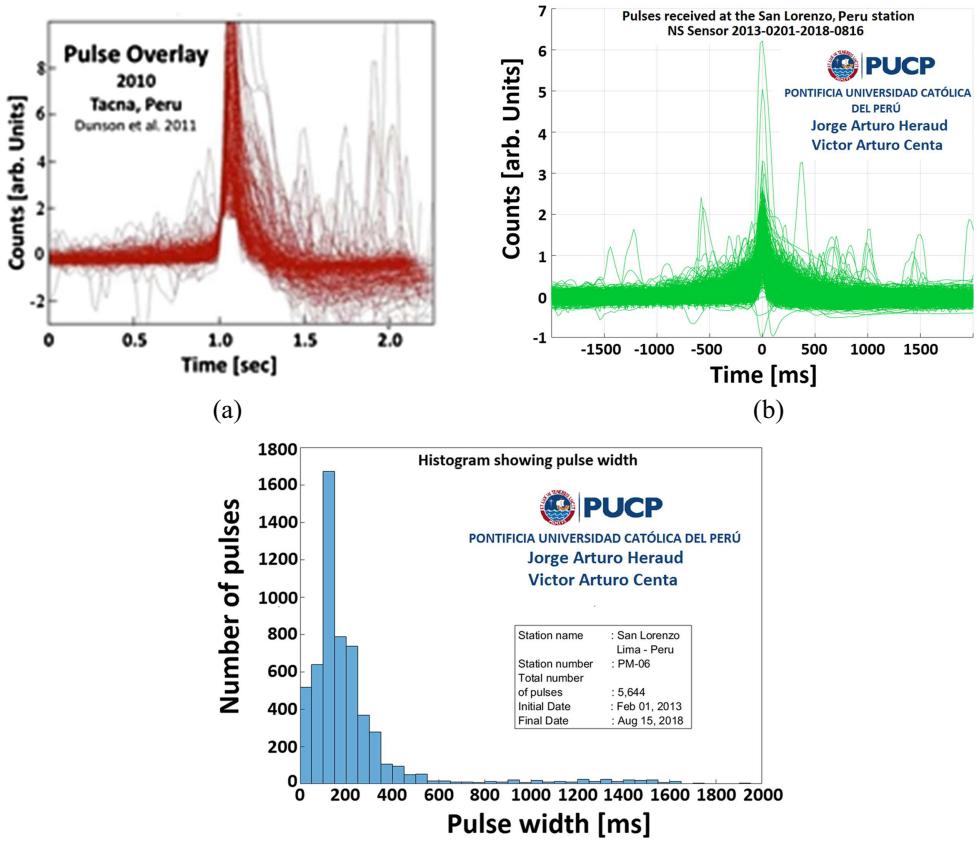

Fig. 1. (a) Unipolar pulse profiles recorded at the Quakefinder Tacna Station in southern Peru [32]. (b) Profiles of 5644 pulses recorded at the Quakefinder San Lorenzo Island stations in central Peru. (c) Histogram of 5644 pulses recorded in central Peru by the Quakefinder stations offshore on the San Lorenzo Island and onshore indicating that the majority of the pulses last 100–150 msec.

same location. Recorded from distances up to ∼100 km, the intensity of the pulses reach 1.5 nT [33,34]. Their unipolar nature indicates that they are not emitted by a point source but by linear or planar sources [31], probably at the top of the Benioff Zone, which marks the boundary between the subducting Nazca plate and the South American continent.

Another location where UPs have been recorded is in central Italy prior to the $M = 6.3$ L'Aquila earthquake of April 06, 2009, a strike-slip event with a hypocentral depth of 9.6 km [11,35].

This paper addresses the solid state processes that need to take place to generate the intense and short current bursts necessary to produce UPs.

2 Results and discussion

2.1 Rocks as insulators

From an electrical conductivity perspective, the igneous and high-grade metamorphic rocks are insulators with wide band gaps, E_g, 4.5 eV or wider. With such large E_g values the probability to thermally promote electrons from the valence band to the conduction band is negligibly small at temperatures below 600–700°C. Hence, their overall electrical conductivity should be low across a wide temperature range, which includes the temperatures prevailing in most of the Earth's crust [36].

2.2 Peroxy defects

Peroxy defects are point defects in the matrix of minerals, which consist of two tightly bonded oxygen anions in the 1-valence state [37]. Peroxy defects are electrically inactive, so long as their O^-–O^- bond is intact. When the O^-–O^- bond breaks, electronic charge carriers become activated, electrons e' and holes, $h\bullet$. Thus, the activation of peroxy defects generates mobile electronic charge carriers where none existed before [28].

Basic information about peroxy defects has been obtained through a study of melt-grown MgO single crystals of the highest nominal purity grade [38]. The first hint for the presence of peroxy came from a mass spectroscopic study of the dehydroxylation of ultrahigh purity $Mg(OH)_2$, which produced an abnormally large amount of H_2 and evidence for the formation of peroxy anions, O_2^{2-}, decomposing above 600°C by releasing O atoms [39]. A follow-up infrared study of MgO single crystals containing OH^- (due to traces of H_2O dissolved in the crystal matrix) provided evidence that pairs of OH^- in the MgO matrix undergo a redox conversion to O_2^{2-} plus H_2 [40,41]. Additional studies dealt with the temperature-dependent effects of peroxy on various physical properties of MgO single crystals including electrical conductivity, dielectric polarization, and magnetic susceptibility as reviewed in [38].

It was further determined that the short, tight peroxy bond is such a succinct entity that the surrounding matrix, be it MgO, CaO, SiO_2 or silicate minerals, has little effect on the response of O^-–O^- bonds. Therefore, lessons learned from the analysis of O_2^{2-} in MgO can help better understand the response of peroxy bonds in a broad range of rock-forming minerals.

Thermodynamics mandates that, during crystallization from a melt or magma that contains dissolved H_2O, the crystalline matrix of any mineral formed will take up a finite concentration of H_2O, forming a solid solution (ss) as depicted in Figure 2 [42].

When AO is MgO, the incorporation of δ H_2O [43] can be written as:

$$MgO + \delta H_2O \Leftrightarrow Mg_{1-\delta}(OH)_{2\delta}O_{1-2\delta} + \delta MgO \tag{1}$$

In the case of silica, the incorporation of δ H_2O can be formalized as:

$$SiO_2 + \delta H_2O \Leftrightarrow Si_{1-\delta/2}(OH)_{2\delta}O_{1-2\delta} + 1/2\delta SiO_2 \tag{2}$$

Similar equations can be written for any silicate minerals.

By introducing $2\delta OH^-$ into the matrix of MgO, δMg^{2+} vacancies are created. The OH^- are preferentially associated with these cation vacancies:

$$H_2O + O^{2-} \Leftrightarrow OH^- + OH^- \tag{3}$$

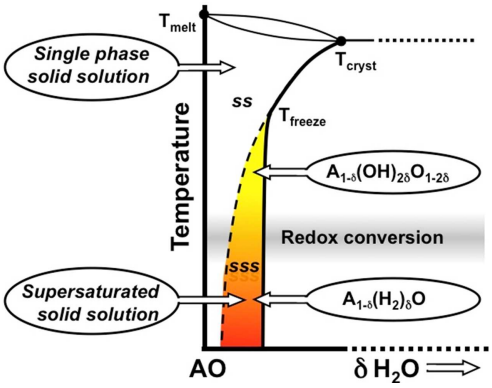

Fig. 2. Phase diagram of a solid AO (oxide or silicate mineral) crystallizing in the presence of H_2O as fluid component.

Likewise, the introduction of H_2O into the matrix of silica or silicates can be written as the hydrolysis of an Si–O–Si bonds, where Si^{4+} may be substituted by Al^{3+} etc.:

$$\mathrm{Si{-}O{-}Si} + \mathrm{H_2O} \Leftrightarrow \mathrm{Si{-}OH\ HO{-}Si} \tag{4}$$

During cooling, so long as the diffusional processes required to exsolve OH^- from the solid matrix can keep up with the cooling rate, the width of the ss field will shrink as indicated in Figure 2. Inevitably, however, a temperature will be reached where thermodynamic equilibrium can no longer be maintained, even at geologically slow cooling rates. This causes the ss to drift out of equilibrium and to turn into a supersaturated solid solution (sss). In the process, the last OH^- that exsolve from the sss grains will become enriched along grain boundaries. In other words, grain boundaries will end up decorated with OH^- or Si–OH.

Upon further cooling, in the sss state, OH^- pairs undergo an electronic rearrangement by way of a redox conversion, in the course of which the two hydroxyl protons take over one electron each from their respective hydroxyl oxygens, changing from H^+ into H, which combine to form H_2. At the same time the two donor hydroxyl oxygens change from O^{2-} to O^-, and the two O^- snap together to form a peroxy bond, O_2^{2-}:

$$\mathrm{OH^-} + \mathrm{OH^-} \Leftrightarrow \mathrm{O_2^{2-}} + \mathrm{H_2} \tag{5}$$

Basically, this redox conversion is reversible. However, when the H_2 molecules enter interstitial sites in the solid matrix or otherwise diffuse away, H_2 molecules and peroxy defects become spatially separated. Hence, reactions generating peroxy out of hydroxyl pairs become irreversible and the solid matrices, in which these reactions occur, acquire excess peroxy defects.

Peroxy defects are known to exist in silica [44–46] and apatites [47]. Their behavior as a function of temperature, specifically their thermal break-up [48], is essentially indistinguishable from that of peroxy in the MgO matrix. Likewise, O_3Si–OH pairs in silicate minerals undergo the same redox conversion to O_3Si–OO–$SiO_3 + H_2$, where Si^{4+} may be substituted by Al^{3+} etc. [37]. Figure 3a outlines this reaction scheme, which starts by an H_2O hydrolyzing a O_3Si–O–SiO_3 bond and subsequently undergoing a redox conversion to peroxy, O_3Si–OO–SiO_3, plus an H_2 molecule.

Peroxy defects are electrically inactive as long as their O^-–O^- bonds are intact. Their temperature-driven break-up occurs in two stages, which have been studied in detail for O_2^{2-} in the MgO matrix at ambient pressure [38]. The process begins with loosening the tightly bound spins in the O_2^{2-} entity, which remain at first in

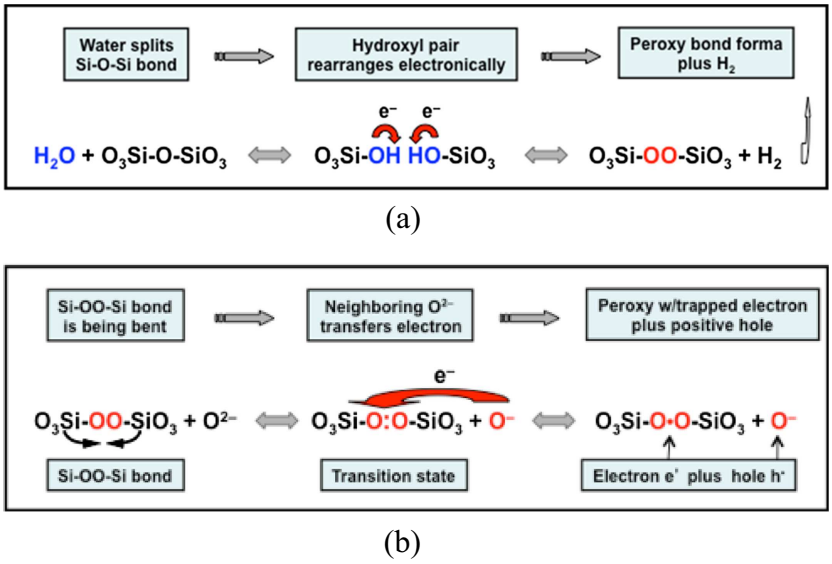

Fig. 3. (a) Introduction of peroxy defects into a silicate structure via a 2-step reaction, first H_2O splitting an O_3Si–O–SiO_3 bond to form a O_3SiOH pair, followed by a redox conversion of the O_3SiOH pair to O_3Si–OO–SiO_3 plus molecular H_2. (b) Activation of a peroxy bond in a silicate matrix via a 2-step process leading to electron-hole pairs on the oxygen sublattice.

a diamagnetic, antiparallel spin state, then transition to a paramagnetic state, indicating that the electron spins have started to flip while still remaining bound to the peroxy site. This first step is called "decoupling", a designation that will be used throughout the present paper. After decoupling, the O^-–O^- bond can dissociate, generating electrons e' and holes h• as highly mobile charge carriers. This 2-stage reaction scheme is depicted in Figure 3b. In accordance to the point defect convention [49] the two holes, O^-, in the decoupled peroxy bond are designated by dots **:**. Next an electron e' from a neighboring O^{2-} is transferred into the decoupled peroxy bond, where it becomes trapped. Thus, the number of holes in the former peroxy bond is reduced from two to one, •, while the donor O^{2-} turns into O^-, equivalent to an unbound hole h•:

In semiconductor parlance, an O^- in a matrix of O^{2-} represents a defect electron or hole h•. Thus, the two holes in O_2^{2-} or Si–OO–Si can be described as self-trapped hole pairs in the oxygen anion sublattice. The peroxy entity is characterized by a short O^-–O^- bond, <1.5 Å as compared to the regular O^{2-}–O^{2-} bond distances of 3.0 Å in MgO [50] and ∼2.8 Å in silicates. Thus, the volume occupied by two O^- in a peroxy bond is much smaller, about 1/8th, the volume of two O^{2-}. This large partial molar volume difference will play an important role in the subsequent discussion.

2.3 Volume changes during break-up of peroxy bonds

Information about the thermal 2-stage break-up of peroxy bonds has been obtained by studying using melt-grown MgO single crystals, nominally 99.99% pure. Specifically, the study focused on the following properties:

- Distribution of OH^- in the MgO matrix [40],
- Electrical conductivity [51],
- Linear expansion [52]

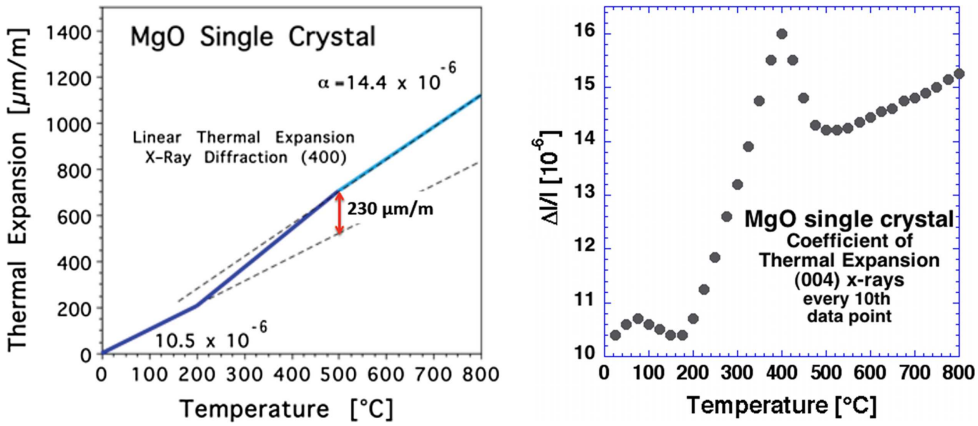

(a) (b)

Fig. 4. (a) Linear thermal expansion in μm/m of an MgO single crystal measured by means of the 004 Bragg reflection, recorded at 1 bar pressure. (b) Derivative of the linear thermal expansion of the MgO crystal at 1 bar as derived from the 004 Bragg reflection.

- Magnetic susceptibility [53,54]
- Dielectric polarization [38].

Figure 4a shows the thermal expansion in μm/m of an MgO single crystal recorded via its 004 Bragg reflection [55][1]. Given the simple cubic structure of MgO, nominally high purity 99.99%, and the absence of any phase transition in MgO [56], the Debye theory applies. Hence, the thermal expansion of MgO at ambient pressure, 100 kPa, should be smooth, without any discontinuities [57,58]. However, as Figure 4a demonstrates, the thermal expansion of the MgO exhibits remarkable discontinuities, for which there is only one possible explanation: though listed as 99.99% pure the MgO crystal under study must contain impurities or imperfections that are not included in the nominal purity rating. These impurities or imperfections could be either

1. low-z elements H, C, and N, which derive from gas/fluid phase components or
2. deviations from the stoichiometric 1:1 Mg:O ratio.

Figure 4b shows the thermal expansion coefficient $\Delta l/l$ of MgO, plotting only every 10th data point. The slightly unstable response in the low temperature range is due to chemisorbed water on the MgO surface. Other noteworthy features are:

(1) increase of the $\Delta l/l$ starting at 180°C, indicating an accelerated volume increase,
(2) decrease of the $\Delta l/l$ between 430°C and 500°C, indicating a decrease in volume, and
(3) resumption of the $\Delta l/l$ increase above 500°C with a slightly larger linear coefficient.

These changes in thermal expansion, in particular at 180–200°C and 400–430°C, correlate with changes in electrical conductivity [51], magnetic susceptibility [53] and dielectric polarization [38], suggesting that they are all linked. The most likely cause are peroxy defects in the MgO matrix, introduced via the dissolution of small amounts of H_2O during crystallization from a slightly H_2O-laden melt.

The discontinuities in the thermal expansion response noted in Figure 4a and 4b are due to the 2-stage break-up of peroxy defects: Step I begins at about 200°C and

[1] The recorded points are so closely spaced that they appear to form a continuous line.

leads to a volume increase that accelerates up to 400°C, followed by a transition between 400°C and about 460°C. Step II begins around 430°C and extends to at least 800°C. Given the low concentration of peroxy defects, <1000 ppm, the $\Delta l/l$ increase is unusually large, in particular between 180°C and 400°C. No measurable broadening of the 004 x-ray reflection was observed as would be expected, if the volume expansion were caused by strain halos around some unspecified point defects [59].

The information provided by the thermal expansion [52], electrical conductivity [51], and magnetic susceptibility [53,54] measurements combines to indicate the 2-stage activation of peroxy defects in the MgO matrix as presented in Figures 3a and 3b:

Step I: decoupling of the O^-–O^- bond without activating mobile charge carriers;
Step II: dissociation of the O^-–O^- bond and generation of mobile charge carriers.

The absence of strain broadening of the x-ray reflection [28] is consistent with the thermal expansion anomaly not being caused by local strains developing around point defects but by slightly increased interatomic distances. This in turn is consistent with a wide delocalization of the wave function during Step I, spreading over many neighboring O^{2-}. The sharp $\Delta l/l$ drop at 400°C in Figure 4b marks the on-set of the peroxy dissociation, generating mobile charge carriers. These charge carriers lead to an increase in electrical conductivity by up to 6 orders of magnitude [60]. In conclusion, when peroxy defects decouple, the overall volume of the MgO increases, but when the peroxy defects dissociate, the volume decreases again.

2.4 Electronic wave function associated with the hole states

To understand why the break-up of the peroxy bond leads to a volume increase, we consider the fact that, when the wavefunction of a hole states delocalizes over many O^{2-} neighbors, the valence band electron density of all those O^{2-} decreases. This decrease reduces the Coulomb interaction between the O^{2-} and their cation neighbors. Since the Coulomb interaction contributes a large portion of the lattice energy, about 90% in MgO [61], any decrease in electron density at the O^{2-} site will weaken the Mg^{2+}–O^{2-} bonds and increase the average Mg^{2+}–O^{2-} distance. Hence, the thermal expansion coefficient must increase [62].

The upper part of Figure 5 depicts the electronic changes believed to accompany the activation of a peroxy defect, O_2^{2-}, in the MgO matrix during Step I and II. The top left panel shows the intact O_2^{2-}, consisting of two tightly coupled O^- that remain coupled up to about 180°C. The center panel depicts the decoupling of the peroxy bond during Step I with both holes still tied to the Mg^{2+} vacancy up to 430°C. The right panel shows the dissociation into an electron trapped at the Mg^{2+} vacancy site, also known as a V^- center [63], plus an unbound and, hence, mobile hole in the O^{2-} sublattice, to which the name "positive hole" has been given [64]. The lower part of Figure 5 illustrates the volume changes that accompany this 2-stage break-up of the peroxy defect, disregarding the effect of temperature. The important point is that the volume expansion during Step I, "decoupling", is followed by a volume contraction during Step II, "dissociation".

The right panel depicts Step II, the dissociated state, which begins around 430°C by an electron transferring from a neighboring O^{2-} into the Mg^{2+} vacancy site, causing the donor O^{2-} to turn into O^-. This O^- constitutes an unbound defect electron in the O^{2-} sublattice, known as a "hole", $h^\bullet$. This $h^\bullet$ is a mobile charge carrier that contributes to the increase in electrical conductivity by several orders of magnitude [51]. Importantly, during Step II, the volume contracts again as indicated in the bottom panel of Figure 5.

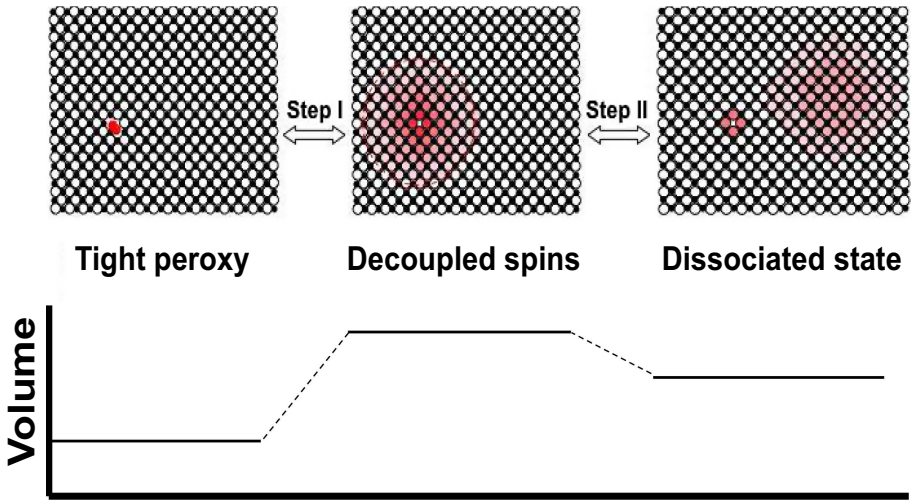

Fig. 5. Top: Two–step break-up of a peroxy defect, here represented in the (100) plane of MgO by first decoupling and delocalizing their electron function, then by dissociating into a trapped hole at the Mg^{2+} vacancy site alongside a mobile positive hole charge carrier. Bottom: Attendant volume change during 2-step break-up of a peroxy defect.

Obviously, since step I is accompanied by a volume (V) expansion, the effect of an externally applied pressure (P) will be to prevent this transition or delay it to a higher temperature (T). Hence, even though the exact V–T–P relationship is unknown, the temperature, at which the O^-–O^- bonds of peroxy defects decouple, is expected to increase with the overload pressure, i.e. with increasing depth in the Earth's crust.

2.5 Molecular orbital approach

Insight may be gained by considering the changes in the Molecular Orbitals (MO), which accompany the changes in the electronic states during the Step I and Step II transitions.

In the undissociated O_2^{2-}, taking z as the O^-–O^- bond direction, the highest occupied MOs are the non-bonding orbitals $1\pi_g^x$ and $1\pi_g^y$, which derive from the O $2p_x$ and O $2p_y$ AOs respectively. Because the antibonding $3\sigma_u^*$ MO is unoccupied, the O^-–O^- bond can be short, <1.5 Å compared to the long O^{2-}–O^{2-} distance, ∼3.0 Å [50].

Figure 6 depicts the MO diagram of O_2^{2-}. On the left and right are the atomic orbitals (AO) for O^-, plotted on an arbitrary energy scale. The center shows the MOs derived from the linear combination of the $O2s^2$ and $O2p^4$ AO's [65]. The two highest MOs of special interest are (i) the fully occupied non-bonding $1\pi_g^x$ and $1\pi_g^y$, orbitals, which are of the same energy and, hence, fourfold degenerate, and (ii) the empty antibonding $3\sigma_u^*$ orbital.

When thermal vibrations increase with increasing temperature, the O^-–O^- bond angles change, causing the $1\pi_g^x$ and $1\pi_g^y$ MOs to shift. In the process their 4-fold degeneracy is lifted, causing the energy of one MO to rise and that of the other MO to decrease. This broadening of the energy levels is a universal, fundamental process. Without loss of generality we depict this process for a peroxy entity in the silica matrix, $O_3Si/^{OO}\backslash SiO_3$ [66]. Figure 7 depicts at the top how the MO's of

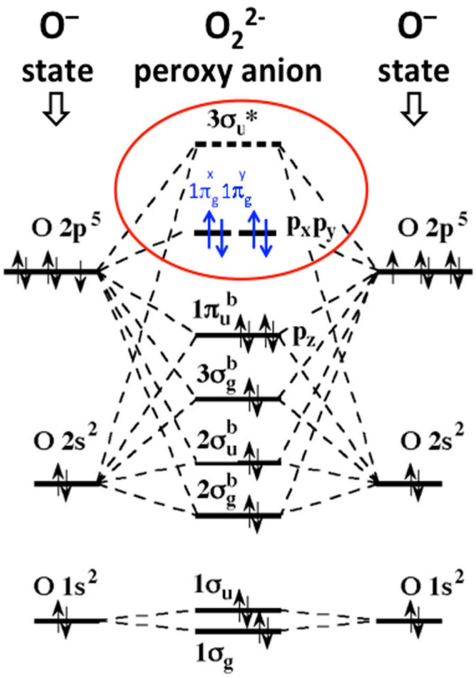

Fig. 6. Molecular orbital diagram of the peroxy anion, O_2^{2-}, as it applies to a high-symmetry lattice environment such as MgO. Importantly, the highest energy level, the antibonding σ^*-type level, is empty, allowing the $O^- - O^-$ bond to be very short.

$O_3Si/^{OO}\backslash SiO_3$ evolve, when the bond angle α changes. For the sake of simplicity, we keep the same symbols as for O_2^{2-} in the cubic MgO lattice environment.

Figure 7 depicts at the top two MO levels for a peroxy defect in a silica or silicate matrix, $O_3Si/^{OO}\backslash SiO_3$. Changing the angle α lifts the 4-fold degeneracy of the $1\pi_g^{nb}$ and $1\pi_g^{nb}$ MO's. It causes the energy of the in-plane MO to be raised and the energy of the out-of-plane MO to be lowered. Inevitably, at some critical angle α, the in-plane $1\pi_g^{nb}$ will cross the antibonding $3\sigma_u^*$ as depicted on the left of the bottom of Figure 7. This forces the two electrons from the non-bonding π^{nb}-type MO to transition into the antibonding $3\sigma_u^*$ MO. As a result, electron density that had resided in the tight torus surrounding the axis of the O^-–O^- bond is now moved to the antibonding region. This causes the O^-–O^- bond distance to increase from the very short peroxy value, <1.5 Å, to a value closer to that of typical distances between O^{2-}, 2.8–3.0 Å. As the distance between the two oxygen nearly doubles, the volume of the two oxygens will increase by a factor of nearly $2^3 \sim 8$.

The π^{nb}–σ^* transition is a second order reaction and begins to be noticeable around 180°C in MgO, reaching its full effect around 430°C, when dissociation sets in. The π^{nb}–σ^* transition is accompanied by a delocalization of the wave function associated with the σ^* level as depicted in the middle panel at the top of Figure 5. About midway during this temperature-driven transition, the magnetic susceptibility of MgO begins to change from diamagnetic to paramagnetic [53,54], indicating that the electron spins in the $3\sigma^*$ level start to flip. During this time, the O^-–O^- bond still holds and no charge carriers are generated that would increase the electrical conductivity.

The right of Figure 7 illustrates Step II, when an electron e' from an outside O^{2-} transfers into the decoupled O^-–O^- bond, initiating dissociation. The donor

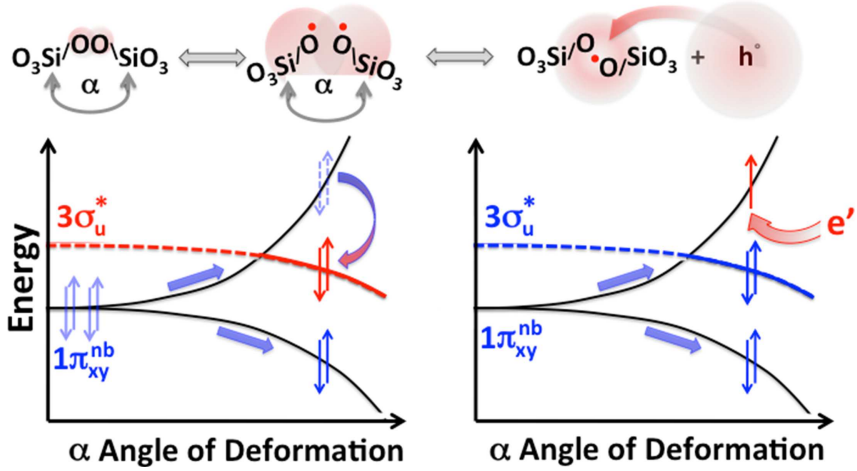

Fig. 7. Representation of the two highest MO levels of O_3 Si/^{OO}\ SiO_3 during deformation of the peroxy bond angle α. The non-bonding 4-fold degenerate π-type level will split. At a critical value of α, one π-type MO will cross the antibonding σ^* level, causing two electrons to be transferred from the non-bonding π-type to the antibonding σ-type level. For the sake of illustration, we keep the π and σ designation as for O_2^{2-} in the high symmetry cubic environment.

O^{2-} thereby turns into O^-. Such an O^- represents a defect electron in the O^{2-} sublattice, a positive hole, a highly mobile h• charge carrier. Hence, Step II marks the steep increase in electrical conductivity observed at 430°C [51]. Importantly, as depicted in Figure 4b, 430°C also marks the midpoint of the decrease of the thermal expansion coefficient in the 400–460°C window, followed – upon further heating – by an increase of $\Delta l/l$, consistent with the dissociation following second order kinetics.

2.6 Peroxy activation by stress

So far, temperature was the variable that causes the break-up of the peroxy bonds. However, peroxy defects can also be activated by stress, specifically by deviatoric stresses [67]. In fact, in rocks, deviatoric stresses are highly effective already at small to very small stress levels to activate h• charge carriers [24]. The reason is that peroxy defects tend to accumulate along grain boundaries or even straddle grain boundaries. This makes them highly susceptible to even slight displacements of the mineral grains relative to each other, causing the peroxy bond angles α to change as depicted in Figure 7. Thus, during mechanical activation, Step I (decoupling) and Step II (dissociation) tend to merge into a single unresolved step creating e' and h• charge carriers. Thus, two processes take place simultaneously: (i) e' and h• charge carriers inside the stressed subvolume recombine, reconstituting peroxy bonds, and (ii) h• charge carriers are able to flow out of the stressed subvolume, spreading into surrounding less stressed or unstressed rocks [24].

Even on a microscopic scale, during activation by stress, peroxy defects still have to decouple their O^-–O^- bonds before they can dissociate. According to Figure 5 decoupling of the peroxy bond is accompanied by a volume increase. This has to be taken into account, when a rock subvolume is stressed under confining pressure in the rock column. To address this aspect, we consider volume changes during Step I and II at constant temperature in the $(P–V)_T$ plane.

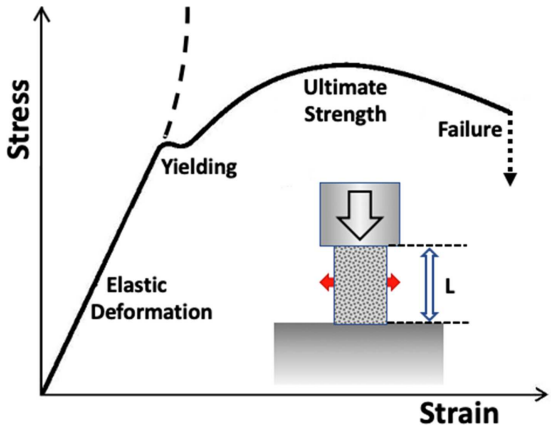

Fig. 8. Generic stress–strain curve during deformation of a brittle material such as a rock. Solid line: stressing an unconstrained rock volume that can expand (red arrows). Dashed line: Stressing a rigidly confined rock volume that cannot expand. https://www.instructables.com/id/Steps-to-Analyzing-a-Materials-Properties-from-its

2.7 Volume instability during peroxy activation

In laboratory tests, it is common practice to stress unconfined axially loaded rock cylinders until failure. Their typical stress-strain response is shown by the solid curve in Figure 8 [68]. Initially, within the range of Hooke's Law, stress rises linearly with strain. After "yielding", the rock cylinder begins to plastically deform, passing through a point of ultimate strength before reaching the point of failure. Throughout this time the total volume increases ever so slightly and the stress-strain curve is convex.

By contrast, if the rock volume under consideration is deep in the Earth's crust, its ability to expand is counteracted by the rigidity of the surrounding rocks [69]. As the confining rocks resist the volume expansion, the stress increases rapidly without increase in strain. Hence, the stress-strain curve becomes concave as indicated by the dashed line in Figure 8.

Eventually the slope of the dashed portion of the stress-strain curve in Figure 8 will become infinite, causing the $\pi^{\mathrm{nb}} -> \sigma^*$ transition and its attended volume expansion to take place against the confining pressure. At the same time, mobile charge carriers, e' and $\mathrm{h}\bullet$, become available. As they flow out, the volume will contract again as indicated in Figure 5.

2.8 Current outbursts from a confined rock volume

Figure 9 transcribes this sequence of events into the volume–pressure $(\mathrm{V–P})_{\mathrm{T}}$ plane. The bold curve marks the boundary between the stability fields of the undissociated and dissociated peroxy states. Point 1 represents the V–P conditions for rock at a given depth. If peroxy defects try to make the transition according to Step I, the compressibility of the confining medium will counteract the volume expansion by an increase in pressure until point 2 is reached. At point 2, if enough peroxy defects in the rock are able to achieve the $\pi^{\mathrm{nb}} -> \sigma^*$ transition, the delocalization of their electronic wave functions can create a situation, where their wave functions overlap, creating a plasma state. In this moment a new force comes into effect: the electron degeneracy pressure, which can overwhelm any confinement pressure. This will cause

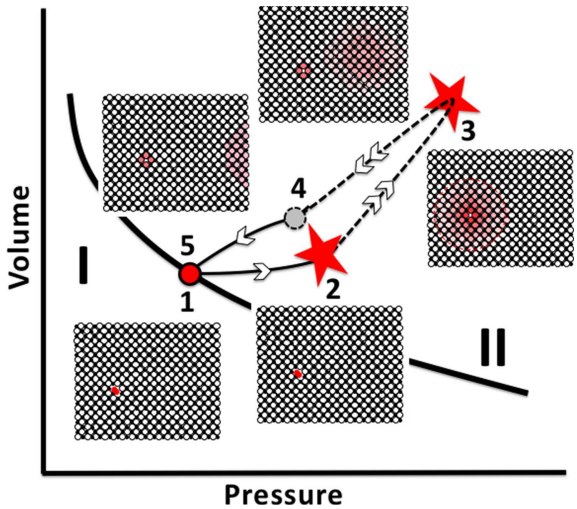

Fig. 9. Sequence of steps leading to a volume instability in the Volume-Pressure plane at constant temperature T. The bold line marks the boundary between undissociated and dissociated peroxy defects. The arrow from 1 to 2 marks the small volume and large pressure increase, when the peroxy are prevented by the build-up of pressure to initiate decoupling. The double arrows from Point 2 to 3 and 4 mark the very rapid transition to the decoupled and dissociated stages marked by the outburst of charge carriers. Point 5 marks the return to a stable state.

the volume to expand explosively along the dashed line from Point 2 to Point 3 (upper red star). At Point 3, the peroxy defects achieve Step I, the decoupled state. This state will be instantly followed by dissociation, i.e. by Step II and the generation of e' and h•. These charge carriers will then burst out of the subvolume causing a very rapid volume contraction from point 3 to point 4, followed by somewhat slower volume contraction to point 5, as the system returns to equilibrium.

The explanation offered in Figure 9 is consistent with the shape of the unipolar pulses as documented in Figure 2, which suggests that a backflow of some charge carriers after their explosive outflow[2]. This backflow is expected to produce an EM signal of opposite polarity and longer duration during the path from Point 4 to Point 5.

Figure 10 projects the same sequence of steps onto the Volume–Time plane. While it may take a long time for the system to go from Point 1 to 2, the time to go from 2 to 4 will be very short, on the order of 150 msec, and moderately short to go from Point 4 to 5, on the order of seconds. This graph qualitatively reproduces the type of unipolar EM pulses observed in the field, namely that they appear out of some random background, rise fast and decay nearly as fast, typically within 150 ms, with an overshoot that can last for 1–2 sec [32,70], sometimes as long as 10–20 sec [35,71], returning to equilibrium.

2.9 Plasma state of the emitting rock volume

The speed with which h• charge carriers can propagate through rocks has been experimentally determined: 100–200 m/sec [72], a speed that is consistent with

[2] The outflow of h creates a charge imbalance, which may be internally balanced by an in situ oxidation of transition metal cations such as $Fe^{2+} + O^{-} => Fe^{3+} + O^{2-}$.

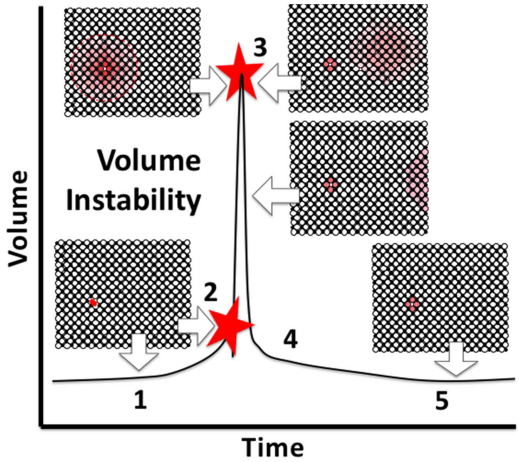

Fig. 10. Sequence of events plotted in the volume-time plane at constant temperature. The time axis is non-uniform: very long from Point 1 to 2, very short from Point 2 to 4 and moderately short from Point 4 to 5.

phonon-assisted electron hopping [73]. However, if UPs were generated by an outburst of only h• charge carriers produced via this mechanism, it becomes difficult to understand how this process can lead to EM pulses as short as 150 msec and as powerful as suggested by the strength of the EM signals recorded at the Earth's surface [30]. In 150 msec, h• charge carriers propagating between 100–300 m/sec would be able to travel just 15–45 m, which is probably not enough to create such strong EM signals.

At this point the above-mentioned study becomes important during which a subvolume of gabbro was stressed at different stress rates from slow to fast, varying over 8 orders of magnitude into the subsecond range [28]. The results indicate that the higher the stress rate, the more e' and h• charge carriers are activated and the more h• become available to flow out of the stressed subvolume. This observation may be combined with the fact that the wave functions of the electronic charge carriers activated during stressing will be highly delocalized. This means that, if the number density of the charge carriers is high enough, the wave functions will overlap [74], creating a solid state plasma. This will generate an electron degeneracy pressure that can overpower any confining presssure [75] and lead to a forceful volume expansion. In the solid state plasma state, however, the outburst speed will no longer be limited by the phonon-mediated electron hopping mechanism peoposed for the h• outflow [76]. Instead the outburst speed can be expected to be much faster, possibly approaching the speed of light in the dielectric medium [77].

The majority of the UPs from Tacna in the south of Peru and most of the UPs recorded over the course of 5 1/2 years at the San Lorenzo station near Lima, Peru, are 150 msec long and exhibit nearly identical profiles as illustrated in Figure 2a–2c. This indicates that, even though the pulses recorded at the San Lorenzo station are emitted from different patches aligned along the Benioff Zone of the subducting Nazca Plate between 25 and 65 km depth [71], they are almost identical with respect to duration and halfwidth. This supports the fundamental concept presented here, namely that the outburst starts with a transition of the stressed rock subvolume from an insulating state to a solid state plasma state, allowing both electrons e' and holes h• expand very fast into the surrounding rocks. Neither the size of the rock subvvolumes going through this dramatic process nor their depth within the Earth's

crust appear to be sensible parameters. Further studies will be needed to capture the same EM pulses from different directions to derive more information about this remarkable process.

3 Conclusions

UPs have been observed in seismically active regions, notably California [10], Italy [35], and Peru [33,70,78]. They typically last for 150 msec and are characterized by a rapid rise of the EM intensity of one polarity and a slightly slower decay, often followed by an overshoot into the opposite polarity, plus oscillations that can last from 1–2 sec to as long as 10–20 sec.

The mechanism for the generation of UPs as proposed here is based on the recognition that rocks, particular igneous and high-grade metamorphic rocks, appear to be laden with peroxy defects, e.g. pairs of oxygen anions in the valence state 1– that form very short, tight O^-–O^- bonds such as in O_3Si–OO–SiO_3 [37]. Mafic rocks of the gabbro-basalt family are believed to be particularly rich in peroxy defects. Many peroxy links are expected to locate on grain boundaries or even straddle grain boundaries. As long as their O^-–O^- bonds are in a tightly coupled state, they are electrically inactive. However, they are highly susceptible to changes in their bond angle. When rocks are stressed, the O_3Si–OO–SiO_3 bond angles of peroxy defects straddling grain boundaries will change, leading to a break-up and the release of electronic charge carriers, electrons e' and holes $h\bullet$ [24].

The break-up of peroxy bonds forces electrons to transition from a non-bonding π-type orbital to an antibonding σ-type orbital [79,80]. This process, called "decoupling", is accompanied by an increase of O^-–O^- bond length from <1.5 Å to about 2.8–3.0 Å and a volume increase by a factor of about 8. In addition, the electronic wave functions associated with the decoupled O^- will delocalize over neighboring O^{2-}. Next, when the O^-–O^- bonds break up, mobile electrons e' and holes $h\bullet$ are generated and the partial molar volume of the former peroxy defect decreases again relative to the decoupled state.

Inside the Earth's crust, rocks are rigidly confined. Any volume expansion of a stressed subvolume such as created by the $\pi^{nb} -> \sigma^*$ transition will lead to an increase in the confining pressure. This in turn will counteract the volume increase and prevent the $\pi^{nb} -> \sigma^*$ transition from taking place. If, however, the strain rate acting on a rock subvolume is constant, the stress rate will increase exponentially activating ever more e' and $h\bullet$. If the rock contains enough peroxy defects so that the wave functions of their stress-activated e' and $h\bullet$ begin to overlap, it will enter a plasma-like state. This creates an electron degeneracy pressure [74] strong enough to overcome any confining pressure. In this point in time, a short-lived volume instability will develop, causing the stressed rock volume to expand explosively. This allows the $\pi^{nb} -> \sigma^*$ transition to take place, followed instantly by the generation of mobile e' and $h\bullet$ charge carriers. These e' and $h\bullet$ charge carriers will burst out of the confined rock volume, creating a short current pulse.

Such a volume instability can explain the emission of unipolar pulses. It should also have seismic signature, a short P wave pulse similar to those produced by underground explosions. While underground explosions always create a cavity that will subsequently collapse [81], the volume instability during the UPs emission process outlined here should be characterized by a singular P wave signature with little reverberations. Maybe UPs are also linked to the audible booms widely reported in the context of seismic activity, often referred to as "earthquake booms" [82]. Since EM waves travel through solid media at the speed of light divided by the effective dielectric constant, while the P waves travel much more slowly, the UPs should produce

a characteristic pattern of arrival times of their EM signals relative to the P waves that should be associated with them.

The basis for this work was laid in the 1980s, when peroxy defects were first identified and characterized with support by the Deutsche Forschungsgemeinschaft to FTF. We thank the late Minoru M Freund for insightful discussions about the delocalization of the electronic wave functions and degeneracy pressure. We thank Thomas Bleier and Quakefinder LLC for providing access to data collected by their 3-axis search coil magnetometer stations.

References

1. M.T. Torabi, M. Fattahi, Iran. J. Geophys. 50 (2019)
2. N.E. Whitehead, Ü. Ulusoy, Earth Sci. Res. J. **19**, 113 (2015)
3. C. Fidani, Nat. Hazards Earth Syst. Sci. **10**, 967 (2010)
4. T.V. Losseva, I.V. Nemchinov, Nat. Hazards Earth Syst. Sci. **5**, 649 (2005)
5. M. Kamogawa, H. Ofuruton, Y.-H. Ohtsuki, Atmos. Res. **76**, 438 (2005)
6. J.S. Derr, Bull. Seismol. Soc. Amer. **63**, 2177 (1973)
7. P. Hedervari, Z. Noszticzius, Ann. Geophys. **3**, 705 (1985)
8. F.T. Freund, J. Scoville, Pure Appl. Geophys. **2019**, 1 (2019)
9. C.-Y. King, Nature **301**, 377 (1983)
10. T. Bleier, et al., Nat. Hazards Earth Syst. Sci. **9**, 585 (2009)
11. P. Nenovski, Acta Geod. Geophys. (2018)
12. L.J. Lanzarotti, Telluric currents: The natural environment and interactionw with man-made systems, in *The Earth's Electrical Environment*, edited by N.R.C.G.S. Committee (National Academies Press, 1986), pp. 232-258
13. R. Shida, Trans. Seismol. Soc. Japan **9**, 32 (1886)
14. M. Becken, P.A.B. Oliver Ritter, U. Weckmann, Nature **480**, 87 (2011)
15. K.N. Kappler, et al., Comput. Geosci. **133**, 104317 (2019)
16. D. Helman, Ann. Geophys. **56** (2013)
17. F. Zencher, M. Bonafede, R. Stefansson, Geophys. J. Int. **166**, 1318 (2006)
18. P.W.J. Glover, Treat. Geophysics, **11**, 89 (2015)
19. A. Revil, J. Colloid Interface Sci. **307**, 254 (2007)
20. L. Valoroso, L. Chiaraluce, C. Collettini, Geology **42**, 343 (2014)
21. D. Zhao, O.P. Mishra, R. Sanda, Phys. Earth Planet. Inter. **132**, 249 (2002)
22. D. Alekseev, A. Kuvshinov, N. Palshin, Earth, Planet. Space **67**, 108 (2015)
23. E.I. Parkhomenko, A.T. Bondarenko, *Electrical conductivity of rocks at high pressures and temperatures* (NASA, Moscow, 1972), p. 212
24. J. Scoville, J. Sornette, F.T. Freund, J. Asian Earth Sci. **114, Part 2**, 338 (2015)
25. C.H. Scholz, *The mechanism of earthquakes and faulting*, 2nd edn. (Cambrdge Univ. Press, Cambridge, UK, 2002), p. 470
26. G. Hayes, T. Crone, *At what depth do earthquakes occur? What is the significance of the depth?* (2018 August 3)
27. J. Kious, R.I. Tilling, *This dynamic earth: the story of plate tectonics*, in *USGS Unnumbered Series* (1996)
28. T.E. Battalino, Geophys. Div. Code 3253 Naval Air Warfare Center, et al., *Electric air mills*
29. A.V. Guglielmi, Izvestiya Phys. Solid Earth **42**, 179 (2006)
30. J. Bortnik, et al., Ann. Geophys. **28**, 1615 (2010)
31. K.-J. Kim, et al., [arXiv: physics/0003064v2] (2000)
32. J.C. Dunson, S.R.T.E. Bleier, J. Heraud, C.H. Alvarez, A. Lira, Nat. Hazards Earth Syst. Sci. **11**, 1 (2011)

33. J.A. Heraud, et al. Determining Future Epicenters by Triangulations of Magnetometer Pulses in Peru, in *AGU Fall Meeting* (AGU, San Francisco, CA, 2013)
34. J.A. Heraud, V.A. Centa. Triangulation of Pulses of Electromagnetic Activity to Determine When and Where Earthqaukes will occur in Central Peru, in *4th Bi-Annual International Geo-Hazards Research Symposium* (IGRS, NASA Ames Research Park, 2014)
35. P. Nenovski, C.R. Acad. Sci. **69**, 775 (2016)
36. E.I. Parkhomenko, Rev. Geophys. Space Phys. **20**, 193 (1982)
37. F.T. Freund, M.M. Freund, J. Asian Earth Sci. **2015**, 373 (2015)
38. F. Freund, M.M. Freund, F. Batllo, J. Geophys. Res. **98**, 22209 (1993)
39. R. Martens, H. Gentsch, F. Freund, J. Catal. **44**, 366 (1976)
40. F. Freund, H. Wengeler, J. Phys. Chem. Solids **43**, 129 (1982)
41. F. Freund, H. Wengeler, R. Martens, Geochim. Cosmochim. Acta **46**, 1821 (1982)
42. G.R. Rossman, Phys. Chem. Miner. **23**, 299 (1996)
43. M.M. Abraham, C.T. Butler, Y. Chen, J. Chem. Phys. **55**, 3752 (1971)
44. A.H. Edwards, W.B. Fowler, Phys. Rev. B Solid State **26**, 6649 (1982)
45. E.J. Friebele, et al., Phys. Rev. Lett. **42**, 1346 (1979)
46. D. Ricci, et al., Phys. Rev. B **64**, 224104 1 (2001)
47. P.E. Kazin, et al., ChemInform **43**, 32 (2012)
48. F. Freund, M.M. Masuda, J. Mater. Res. **6**, 1619 (1991)
49. F.A. Kröger, *The chemistry of imperfect crystals* (North-Holland Publisher, Amsterdam, 1964)
50. O.E. Taurian, M. Springborg, N.E. Christensen, Solid State Commun. **55**, 351 (1985)
51. H. Kathrein, F. Freund, J. Phys. Chem. Solids **44**, 177 (1983)
52. H. Wengeler, F. Freund, Mater. Res. Bull. **15**, 1241 (1980)
53. F. Batllo, et al., J. Appl. Phys. **67**, 5844 (1990)
54. F. Batllo, et al., J. Appl. Phys. **69**, 6031 (1991)
55. F. Freund, E.J. Whang, J. Lee, Highly mobile hole charge carriers in minerals: Key to the enigmatic electrical earthquake phenomena?, in *Electromagnetic Phenomena Related to Earthquake Prediction*, edited by F. Fujimori, M. Hayakawa (Terra Sci. Publ. Co., Tokyo, 1994), pp. 271–292
56. N. Munjal, et al., Study of phase transition and cohesive energy in MgO, in *Journal of Physics: Conference Series* (2012)
57. A.K. Jonscher, *Dielectric relaxation in solids* (Chelsea Dielectrics Press, London, 1983), p. 380
58. C. Kittel, *Introduction to solid state physics*, 7th edn. (Wiley, New York, 1996)
59. D. Balzar, J. Res. Nat. Inst. Stand. Technol. **98**, 321 (1993)
60. P.K. Abraitis, R.A.D. Pattrick, D.J. Vaughan, Int. J. Mineral Proc. **74**, 41 (2004)
61. G. Pacchioni, et al., Phys. Rev. B. **48**, 11573 (1993)
62. C.Y. Ho, R.E. Taylor, *Thermal Expansion of Solids* (ASM International, Materials Park, OH, 1998)
63. B. Henderson, J.E. Wertz, *Defects in the Alkaline Earth Oxides* (Taylor & Francis, London, 1977)
64. D.L. Griscom, Glass Sci. Technol. **4B**, 151 (1990)
65. E.-H. Chen, T.-C. Chang, J. Molec. Struct. Theochem. **431**, 127 (1998)
66. D. Ricci, et al., Phys. Rev. B **64**, 224104-1 (2001)
67. F.T. Freund, Nat. Hazards Earth Syst. Sci. **7**, 1 (2007)
68. A.P. Boresi, R.J. Schmidt, O.R. Sidebottom, *Advanced Mechanics of Materials* (Wiley, 1993)
69. H. Kimizuka, et al., Phys. Rev. B **75**, 054 (2007)
70. J. Scoville, J. Heraud, F. Freund, Nat. Hazards Earth Syst. Sci. Discuss. **2**, 7367 (2014)
71. J.A. Heraud, V. Centa, T. Bleier, Electromagnetic Precursors Leading to Triangulation of Future Earthquakes and Imaging of the Subduction Zone. in *AGU Fall Meeting* (AGU, San Franciso, CA, 2015)
72. F. Freund, J. Geodyn. **33**, 545 (2002)
73. D.L. Griscom, Glass Sci. Technol. **48**, 151 (1990)
74. G.K. Schenter, R.L. Liboff, J. Appl. Phys. **62**, 177 (1987)

75. F.J. Dyson, A. Lenard, J. Math. Phys. **8**, 423 (1967)
76. T. Toulkeridis, et al., J. Geodyn. **126** (2019)
77. C.A. Balanis, *Advanced engineering electromagnetics* (Wiley, 2012), p. 1040
78. J. Scoville, J. Heraud, F. Freund, [arXiv: 1405.4482] (2014)
79. C.G. Dodd, G.L. Glen, J. Appl. Phys. **39**, 5377 (1968)
80. G. Frenking, S. Shaik, *The Chemical Bond. Fundamental Aspects of Chemical Bonding* (John Wiley, 2014), p. 438
81. T.V. McEvilly, W.A. Peppin, Geophys. J. Int. **31**, 67 (1972)
82. USGS, *Earthquake Booms, Seneca Guns, and Other Sounds* (2018), Available from: https://earthquake.usgs.gov/learn/topics/booms.php